"5th International Symposium on Refined Flow Modelling and Turbulence Measurements", Paris, Sep 7-10. 1993.

Lars DAVIDSON
Thermo and Fluid Dynamics
Chalmers University of Technology
S-412 96 Gothenburg, Sweden

HIGH LIFT AIRFOIL FLOW SIMULATIONS USING A TWO-LAYER REYNOLDS STRESS TRANSPORT MODEL

ABSTRACT

A second-moment Reynolds Stress Transport Model (RSTM) is used in the present work for computing the flow around a two-dimensional airfoil. An incompressible SIMPLEC code is used, employing a non-staggered grid arrangement. A third-order QUICK scheme is used for the momentum equations, and a second-order, bounded MUSCL scheme is used for the turbulent quantities. As the RSTM is valid only for fully turbulent flow, an eddy viscosity, one-equation model is used near the wall. The two models are matched along a pre-selected grid line in the fully turbulent region.

Detailed comparisons between calculations and experiments are presented for an angle of attack of $\alpha = 13.3^o$. The RSTM predictions agree well with the experiments, and approaching stall is predicted for $\alpha = 17^o$, which agrees well with experimental data. The results obtained with a two-layer $k - \varepsilon$ model show poor agreement with experimental data; the velocity profiles on the suction side of the airfoil show no tendency of separation, and no tendency of stall is predicted.

INTRODUCTION

Flow around airfoils is an interesting turbulent flow configuration involving a number of fundamental physical flow phenomena such as transition, curvature-induced production damping of turbulence, separation and wake flow. Transition is usually not predicted but is prescribed from experimental data. Some work has been presented in which transition is predicted using the e^n-method based on the linearized stability theory (Cebeci, 1989). In real (industrial) configurations, it is of utmost importance to be able to predict the locations of transition; in the present study, however, the locations of transition are prescribed from experimental data.

Curvature effects, related either to curvature of the wall or streamline curvature, are known to have significant effects on the turbulence (Bradshaw, 1973). Both types of curvature are present in airfoil flows, the former on the suction side and the latter in and near the separation region. The entire Reynolds tensor is active in the interaction process between shear stresses, normal stresses and mean velocity strains. When predicting flows where curvature effects are important, it is thus necessary to use turbulence models that accurately predict all Reynolds stresses, not only the shear stresses.

Second-moment closures such as RSTM are superior to simpler turbulence models such as the $k - \varepsilon$ or the Baldwin-Lomax models. The main reasons for their superiority are their ability to account for *i)* streamline curvature, *ii)* strong nonlocal effects and history

effects for the individual stresses and *iii)* irrotational strains, phenomena which all are present in airfoil flow.

NUMERICAL METHOD

The finite volume computer program CALC-BFC (Davidson and Farhanieh 1992) (**B**oundary **F**itted **C**oordinates) for three-dimensional complex geometries is used in this study. The program uses Cartesian velocity components, and the pressure-velocity coupling is handled with the SIMPLEC procedure. Staggered grids for the velocities have been used in most finite volume programs. In the present work, however, a collocated grid arrangement is used, which means that velocities are stored together with all scalar variables such as $p, k, \varepsilon, \overline{u_i u_j}$ at the centre of the control volume. This concept was suggested by Rhie and Chow (1984).

The convective terms in the mean flow equations are discretized using QUICK, a third-order scheme by Leonard (1979). For turbulent quantities ($\overline{u^2}, \overline{v^2}, \overline{uv}, k$ and ε) MUSCL, a second-order, bounded scheme of van Leer (1979), is used.

THE REYNOLDS STRESS TRANSPORT MODEL

The Reynolds Stress Transport Model has the form (Gibson and Younis, 1986):

$$\underbrace{\frac{\partial}{\partial x_k}\left(\rho U_k \overline{u_i u_j}\right)}_{\text{convection}} = \underbrace{-\rho\overline{u_i u_k}\frac{\partial U_j}{\partial x_k} - \rho\overline{u_j u_k}\frac{\partial U_i}{\partial x_k}}_{\text{production } P_{ij}} + \Phi_{ij} + D_{ij} - \rho\varepsilon_{ij} \tag{1}$$

The convection and production terms are exact and do not require any modelling assumptions. The pressure strain Φ_{ij} and the dissipation ε_{ij} are modelled following Gibson and Younis (1986).

The diffusion term D_{ij} can be modelled using the Generalized Gradient Diffusion Hypothesis GGDH (Daly and Harlow, 1970). However, as severe convergence problems were experienced using the GGDH owing to the destabilising cross-derivatives, the diffusion term D_{ij} is modelled using the eddy viscosity assumption. Following a suggestion by Lien (1992), the turbulent Prandtl number σ_t has been modified. The diffusion in the normal direction is usually much more important than in the streamwise direction. The diffusion coefficient using the eddy viscosity formulation is μ_t/σ_t and can be compared with the one in the GGDH-expression, so that

$$\frac{\nu_t}{\sigma_t} \equiv \frac{c_\mu k^2}{\varepsilon\sigma_t} = c_s \frac{k\overline{v^2}}{\varepsilon} \tag{2}$$

With $c_s = 0.22$ and $\overline{v^2}/k \simeq 0.5$, we get $\sigma_t = 0.82$. For ε, we obtain the Prandtl number $\sigma_\varepsilon = 1$ with $c_\varepsilon = 0.18$.

The one-equation model by Chen and Patel (1987), is used near the walls. In this model, the standard k equation is solved and the turbulent length scales are prescribed (see Davidson and Rizzi, 1992).

In an RSTM, there are two equivalent sets of equations which can be solved, either $\overline{u^2}, \overline{v^2}, \overline{w^2}, \overline{uv}$ and ε or $\overline{u^2}, \overline{v^2}, k, \overline{uv}$ and ε. The latter set has been chosen in the present study. The primary reason for this choice is that the k equation must in any case be solved in the one-equation region.

As for the Reynolds stresses, the diffusion terms D^k, D^ε are calculated using the eddy viscosity assumption with $\sigma_k = 0.82$.

BOUNDARY CONDITIONS

At the wall all variables are set to zero except for pressure, for which $\partial^2 p/\partial n^2 = 0$ is

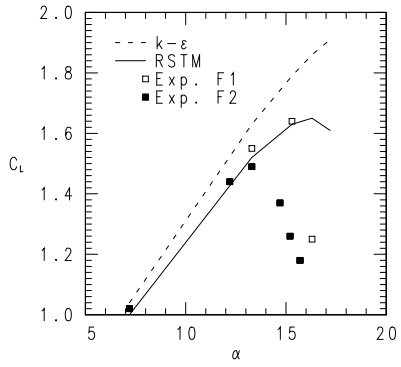

Figure 1: Lift-coefficients C_L versus angle of attack α.

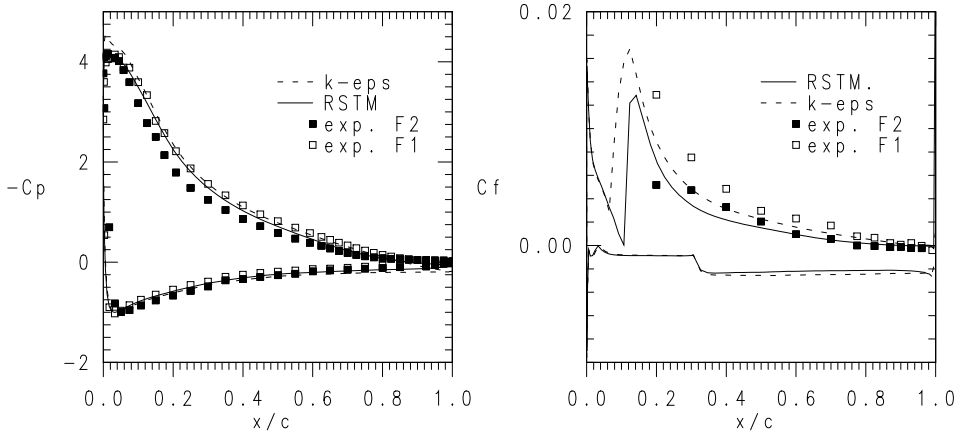

Figure 2: Wall pressure $c_p = (p - p_0)\,/\frac{1}{2}\rho U_0^2$ and skin friction $\tau_w/\frac{1}{2}\rho U_0^2$.

used.

At the farfield the velocity components are set from experimental data, i.e. $U = \cos\alpha$, $V = \sin\alpha$ where α denotes angle of attack. The pressure is set from $\partial^2 p/\partial n^2 = 0$. All turbulent quantities are either set to zero or are extrapolated, depending on whether the case is inflow or outflow.

RESULTS

The results calculated are compared with experimental data taken from Capbern and Bonnet (1989) and Gleyzes (1989). The experimental airfoil is the A-profile, which also was used in the CFD validation EUROVAL project (1993). In Davidson and Rizzi (1992) the flow around this airfoil was computed using an explicit, time-marching Runge-Kutta code, together with an Algebraic Stress Model (ASM). The Reynolds number and the Mach number are 2.1×10^6 and 0.15, respectively. In the calculations, the flow is assumed to be incompressible. Measurements have been carried out in two wind tunnels, F1 and F2. Global characteristics such as friction coefficients and surface pressures were measured in the F1 wind tunnel. The flow field was studied in more detail in the F2 wind tunnel, where mean velocity profiles and Reynolds stresses were measured using a three-component LDV system. The blockage effect in the F2 tunnel was more important than in the F1 tunnel, leading to three-dimensional effects for $\alpha \geq 13^o$.

A C-mesh with 178×96 was used. The near-wall nodes are located at $y^+ \simeq 1$, and 7 to 10 nodes – in the normal direction – are situated in the region $0 \leq y^+ \leq 20$. Another mesh has been tested, in which the number of nodes in the tangential direction to the airfoil was increased by a factor two and where the number of nodes in the normal direction was reduced (353×65). The results obtained with the two meshes differed very little.

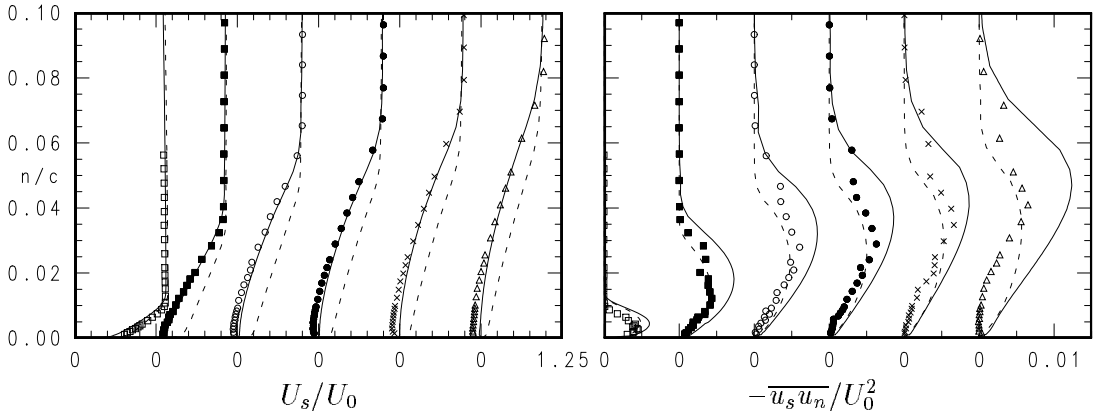

Figure 3: U_n and $\overline{u_s u_n}$ profiles on the suction side of the airfoil. ———, RSTM; – – –, $k-\varepsilon$. □, $x/c = 0.4$; ■, $x/c = 0.775$; o, $x/c = 0.9$; ●, $x/c = 0.93$; ×, $x/c = 0.96$; △, $x/c = 0.99$.

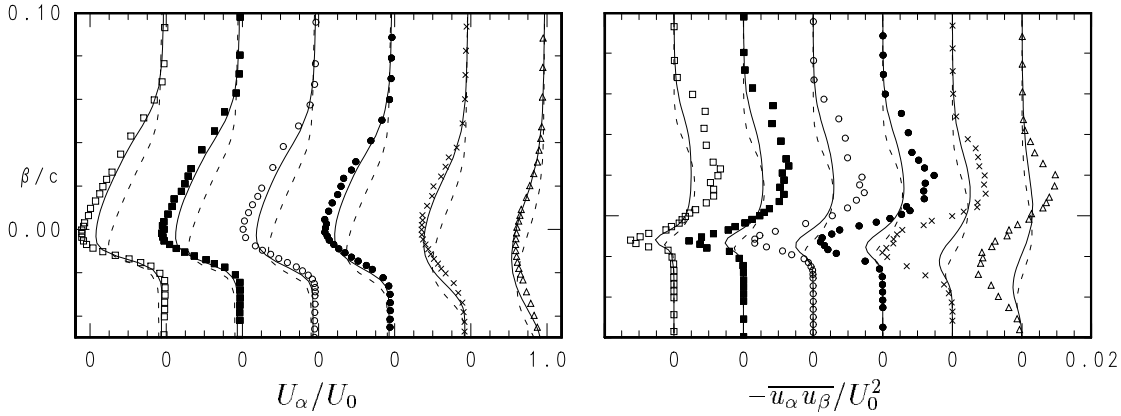

Figure 4: U_α and $\overline{u_\alpha u_\beta}$ profiles in the wake. ———, RSTM; – – –, $k-\varepsilon$. □, $x/c = 1.033$; ■, $x/c = 1.05$; o, $x/c = 1.07$; ●, $x/c = 1.08$; ×, $x/c = 1.15$; △, $x/c = 1.25$.

In Fig. 1 the RSTM-predicted lift-coefficients C_L are compared with $k-\varepsilon$ predictions [two-layer model (Davidson and Rizzi, 1992)] and experimental data. It can be seen that the RSTM agrees well with experiments predicting decreasing C_L at $\alpha = 17^o$, which agrees well with experimental data. However, the $k-\varepsilon$ model shows no tendency to predict stall. It can be seen in Fig. 1 that there is a considerable difference between the experimental results in the two wind tunnels F1 and F2. The results obtained in the larger wind tunnel F1, are considered to be more reliable than those obtained in F2. This should be kept in mind when making detailed comparisons between experimental profiles taken in F2 and calculated results.

The wall pressure and the skin friction are presented in Fig. 2. It can be seen that, with the $k-\varepsilon$ model, the (negative) pressure peak at the suction side is overpredicted as compared with experiments, and that the RSTM predictions agree well with experiments.

The velocity profiles on the suction side of the airfoil are presented in Fig. 3a. Note that an orthogonal $s-n$ coordinate system is used, with origin on the surface. The s coordinate is tangential to the airfoil. The U_s-velocities on the airfoil are well predicted when using the RSTM. A small separation is predicted, occurring at $x/c \simeq 0.90$. This type of separation can be termed *incipient detachment* (Simpson, 1989). As separation is approached, it is seen that the predicted U_s profiles follow the experimental ones, that the profiles become progressively less full and that an inflexion point appears in the profiles. The separation region in the experiments is considerably larger than that in the RSTM-predictions. This may perhaps be attributed to experimental uncertainty in the F2 wind

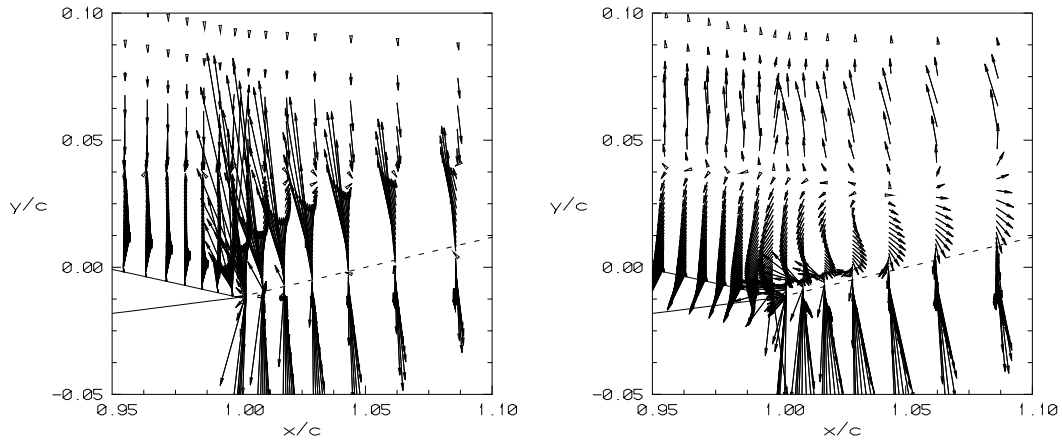

Figure 5a-b: Vector plots of turbulent shear and normal stresses.

	P_{ij}	P^c_{ij}	C^c_{ij}
$\overline{u_r^2}$	-	$2\overline{u_r u_\theta}\,\frac{U_\theta}{r}$	$2\overline{u_r u_\theta}\,\frac{U_\theta}{r}$
$\overline{u_\theta^2}$	$-2\overline{u_r u_\theta}\,\frac{\partial U_\theta}{\partial r}$	-	$-2\overline{u_r u_\theta}\,\frac{U_\theta}{r}$
$\overline{u_r u_\theta}$	$-\overline{u_r^2}\,\frac{\partial U_\theta}{\partial r}$	$\overline{u_\theta^2}\,\frac{U_\theta}{r}$	$(\overline{u_\theta^2}-\overline{u_r^2})\,\frac{U_\theta}{r}$

Table 1: Source terms in the Reynolds stress equations (see Eq.3) due to production and convection in a polar coordinate system

tunnel, because the lift-coefficient in Fig. 1 and the surface pressure data in Fig. 2 indicate that the separation zone in the more reliable measurements in the F1 wind tunnel is smaller. The velocity profiles predicted with the $k-\varepsilon$ model do not agree very well with experiments: no tendency toword separation is observed, which implies that the $k-\varepsilon$ predicts excessively large shear stresses, giving too high a turbulent diffusion and thus smearing out the U_s profiles.

The wake velocity profiles U_α/U_o are compared with experiments in Fig. 4a. Note that an $\alpha-\beta$ coordinate system is used in the wake with origo at the trailing edge; the α axis is parallel to the free-stream velocity, and $\hat{\beta}$ is orthogonal to $\hat{\alpha}$. From Fig. 4a it can be seen that the RSTM shows better performance than the $k-\varepsilon$ model.

The shear stresses on the airfoil and the wake are presented in Figs. 3b and 4b. Using RSTM, the shear stresses are overpredicted, especially near the trailing edge. In the wake, the predicted shear stresses are much smaller than in the experiments, which is probably related to the larger experimental separation zone.

The shear stresses predicted with the $k-\varepsilon$ model are smaller than those predicted with the RSTM, although the velocity profiles in Fig. 3a predicted with $k-\varepsilon$ are fuller than those predicted with RSTM. Normally, a full velocity profile (low form factor H_{12}) is related to large Reynolds stresses. The reason for the shear stresses are higher with RSTM than with $k-\varepsilon$ is that the turbulent quantities were computed with different velocity fields. The velocity gradients in the $k-\varepsilon$ predictions are much smaller than in the RSTM predictions, leading to lower production of turbulence in the former case.

When presenting turbulent quantities such as Reynolds stresses, it may be overlooked that it is not the stresses that enter the momentum equations but their *gradients*, where the Reynolds stresses constitute net (vectorial) forces/area, i.e. net stress vectors. The

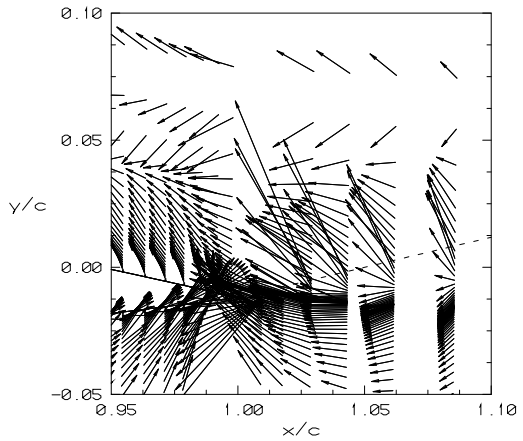

Figure 5c: Vector plots of turbulent stresses and pressure vectors near the trailing edge. The same scaling of vectors is used in all plots. The dashed line has the same direction as the far-field flow ($\alpha = 13.3$). a) $\rho\,(-\partial\overline{uv}/\partial x, -\partial\overline{uv}/\partial y)$, b) $\rho\left(-\partial\overline{u^2}/\partial x, -\partial\overline{v^2}/\partial y\right)$, c) $(-\partial p/\partial x, -\partial p/\partial y)$.

force resulting from shear and normal stresses, $\vec{F}_s$, $\vec{F}_n$, can be written

$$\vec{F}_s = \rho\left(-\frac{\partial\overline{uv}}{\partial x}, -\frac{\partial\overline{uv}}{\partial y}\right),\ \vec{F}_n = \rho\left(-\frac{\partial\overline{u^2}}{\partial x}, -\frac{\partial\overline{v^2}}{\partial y}\right),$$

which should be compared to the force resulting from pressure

$$\vec{F}_p = \left(-\frac{\partial p}{\partial x}, -\frac{\partial p}{\partial y}\right)$$

In Fig. 5, the three force-fields near the trailing edge are presented as vector plots. It can be seen from the pressure force $\vec{F}_p$ that the flow goes against an adverse pressure gradient, both on the airfoil and in the wake. It is interesting to see how the forces (net stress vectors) resulting from to the Reynolds stresses are fairly important in the wake region, especially along the centre line, where the very thin boundary layer from the pressure side mixes with the separated boundary layer from the suction side. Large gradients are formed that give strong downward forces owing to both shear and normal stresses, which are even larger than the forces resulting from the pressure gradient.

As Cartesian velocity components have been used in the calculations, no explicit curvature terms appear in the Reynolds stress equations (see Eq. 1). Of course, the Reynolds stresses formulated in Cartesian coordinates are also affected by curvature, but are affected *implicitly*. To investigate the curvature effects, let us – in the post-processing – study the equations in polar coordinates $r-\theta$, with the flow in the circumferential θ direction (i.e. $U_\theta = U_\theta(r), U_r = 0$). The θ axis is thus chosen so that the flow is *locally* aligned with this axis. Curvature terms now appear because the $r = const.$ coordinate lines are curved. The Reynolds stress equation can, in symbolic form, be written

$$C_{ij} - D_{ij} \;=\; P_{ij} + \Phi_{ij} - \varepsilon_{ij} + P^c_{ij} + C^c_{ij} \tag{3}$$

where superscript c on P_{ij} and C_{ij} denotes curvature terms originating from production and convection, respectively (see Table 1). The larger these terms, the more important the curvature effects.

The flux Richardson number

$$R_f = \frac{2U_\theta/r}{U_\theta/r + \partial U_\theta/\partial r}$$

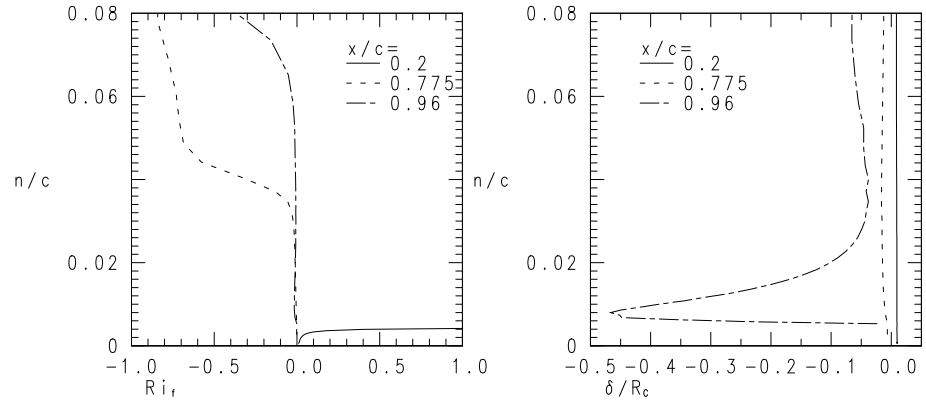

Figure 6: Parameters describing streamline curvature effects on the turbulence. a) Boundary layer thickness over streamline curvature radius δ/R_c. b) Flux Richardson number R_f.

is a convenient parameter for studying curvature effects. Its physical meaning is (minus) the ratio of the production of $\overline{u_r^2}$ owing to curvature to the total production of $\overline{u_\theta^2}$ (see Table 1). The ratio δ/R and the flux Richardson number are shown in Fig. 6 at three different x stations: at $x/c = 0.2$ where the wall curvature is most important, near the separation point ($x/c = 0.775$) and in the separation zone ($x/c = 0.96$). As can be seen, the streamline curvature is positive at $x/c = 0.2$, which in the outer part of the boundary layer gives an increasing flux Richardson number. The flow here is parallel to the curved wall, which gives constant $\delta/R_c \simeq 0.02$, i.e. boundary thickness over wall curvature. The boundary layer is very thin ($\delta/c \simeq 0.005$), which explains the strong increase in the Richardson flux number at $n/c \simeq 0.004$, close to the outer edge of the boundary layer. Further away from the wall $\partial U_\theta/\partial r = \partial U_s/\partial n$ becomes negative (for increasing n, U_s tends towards its free-stream value $U_s = 1$). As separation is approached, the streamlines become concave, which destabilises the turbulence. It is seen in Fig. 6 that δ/R and R_f become negative. The curvature effects are largest in the outer boundary layer, where the curvature term U_θ/R becomes comparable with the velocity gradient $\partial U_\theta/\partial r$. The *direct* influence of the curvature effects are thus largest in the outer part of the boundary layer, but they will also have *indirect* influence via convective and diffusive transport. The Reynolds stresses, augmented or dampened by curvature, increase or decrease the production terms in the equations and, through convection and diffusion, also affect the surroundings. The streamlines bounding the separation region in separated flows are usually convex. It may be noted that, in the present case, the turbulence in the shear layer bounding the separation zone on the suction side is mostly destabilised as a result of the concave curvature of the streamlines. This is because the flow is forced upwards when it reaches the wake, giving concave streamline curvature in the region of the trailing edge.

CONCLUSIONS

The following conclusions can be drawn.

• The RSTM predicts the flow in good agreement with experimental data, and a small separation zone is predicted at $\alpha = 13.3^o$ which could be described as incipient detachment. The computed lift coefficient C_L has a maximum at an angle of attack of 16^o, indicating approaching stall, which is in good agreement with experimental data.

• The $k - \varepsilon$ model predictions are in poor agreement with experiments, the computed flow showing no tendency toward separation at $\alpha = 13.3^o$. No stall is predicted and the lift coefficient continues to increase at $\alpha = 17^o$.

• Curvature effects resulting from wall curvature and streamline curvature are impor-

tant. Computed curvature radii show that the boundary layer thickness over curvature radius is approximately 0.02 ($\delta/R_C \simeq 0.02$) at the suction side close to the pressure minimum. In the region in which the flow approaches the separation region, it is forced further away from the wall. This results in streamlines with a concave curvature; values of δ/R_C close to -0.5 are found.

• When comparing Reynolds stresses one may overlook it is not the Reynolds stresses that appear in the momentum equations but their *gradients*. The (net) stress vectors resulting from shear stresses $\rho(-\partial\overline{uv}/\partial x, -\partial uv/\partial y)$ and normal stresses $\rho(-\partial\overline{u^2}/\partial x, -\partial\overline{v^2}/\partial y)$ are compared with the forces (per unit volume) resulting from the pressure gradient $(-\partial p/\partial x, -\partial p/\partial y)$ in the region of the trailing edge. It is found that the forces that results from both normal stresses and shear stresses are comparable to the forces resulting from the pressure gradient.

REFERENCES

BRADSHAW, P., *AGARDograph*, no. 169, 1973.

CAPBERN, C. and BONNET, Rapport Aerospatiale 443.535./89, Toulouse, 1989.

CEBECI, T., *AIAA J.*, **27**, pp. 1680-1688, 1989.

CHEN, H.C. and PATEL, V.C., AIAA Paper No 87-1300, Honolulu, June 1987.

DALY, B.J. and HARLOW, F.H., *Phys. Fluids*, **13**, pp. 2634-2649, 1970.

DAVIDSON, L. and FARHANIEH, B., Rept. 92/4, Thermo and Fluid Dynamics, Chalmers University of Technology, Gothenburg, Sweden, 1992.

DAVIDSON, L. and RIZZI, A., *J. Spacecraft and Rockets*, Vol. 29(6), pp. 794-800, 1992 (see also AIAA-paper 92-0195, Reno, Jan. 1992).

EUROVAL — W. Haase, F. Brandsma,
E. Elsholz, M. Leschziner and D. Schwamborn (Eds.), Notes on Numerical Fluid Mechanics, Vieweg Verlag (to be published), 1993.

GIBSON, M.M. and YOUNIS, B.A., *Phys. Fluids*, **29**, pp. 38-48, 1986.

GLEYZES, C., Rapport Final ONERA/CERT 57/5004.22, Toulouse, 1989.

HUANG, P.G. and LESCHZINER, M.A., 5th Turbulent Shear Flow, pp. 20.7-20.12, Cornell, 1985.

LEONARD, B.P. — A Stable and Accurate Convective Modelling Based on Quadratic Upstream Interpolation, *Comp. Meth. Appl. Mech. Engng.*, **19**, pp. 59-98, 1979.

LIEN, F.S., PhD thesis, University of Manchester, Manchester, 1992.

LUMLEY, J.L., *Adv. in Appl. Mech.*, **18**, pp. 123-176, 1978.

RHIE, C.M. and CHOW, W.L., *AIAA J.*, **21**, pp. 1525-1532, 1983.

RODI, W. and SCHEUERER, G., *Phys. Fluids*, **26**, No. 6, pp. 1422-1435, 1983.

SIMPSON, R.L., *Ann. Rev. Fluid Mech.*, **21**, pp. 205-234, 1989.

THOMPSON, B.E. and WHITELAW, J.H., *JFM*, **157**, pp. 305-326, 1985.

Van LEER, B., J. Comp. Phys., **32**, pp. 101-136, 1979.